

# CSL-1: chance projection effect or serendipitous discovery of a gravitational lens induced by a cosmic string?

M. Sazhin<sup>1,2</sup>, G. Longo<sup>3,4</sup>, M. Capaccioli<sup>1,3</sup>, J. M. Alcalá<sup>1</sup>, R. Silvotti<sup>1</sup>, G. Covone<sup>4</sup>, O. Khovanskaya<sup>2</sup>, M. Pavlov<sup>1</sup>, M. Pannella<sup>1</sup>, M. Radovich<sup>1</sup>, V. Testa<sup>5</sup>

<sup>1</sup> *INAF - Osservatorio Astronomico di Capodimonte, via Moiariello 16, I-80131 Napoli, Italy*

<sup>2</sup> *Sternberg Astronomical Institute, Universitetsky pr., 13, 119992, Moscow, Russia*

<sup>3</sup> *Dipartimento di Scienze Fisiche, Univ. Federico II, Polo delle Scienze e della Tecnologia, via Cinthia, 80126 Napoli, Italy*

<sup>4</sup> *INAF - Telescopio Nazionale Galileo, Roque de Los Muchachos, Santa Cruz de La Palma, 38700-TF, Spain P.O. Box 565*

<sup>5</sup> *INAF - Osservatorio Astronomico di Monte Porzio, Monte Porzio Catone (Roma) Italy*

14 May 2018

## ABSTRACT

CSL-1 (Capodimonte–Sternberg–Lens Candidate, No.1) is an extragalactic double source detected in the OACDF (*Osservatorio Astronomico di Capodimonte - Deep Field*). It can be interpreted either as the chance alignment of two identical galaxies at  $z = 0.46$  or as the first case of gravitational lensing by a cosmic string. Extensive modeling shows in fact that cosmic strings are the only type of lens which (at least at low angular resolution) can produce undistorted double images of a background source. We propose an *experimentum crucis* to disentangle between these two possible explanations. If the lensing by a cosmic string should be confirmed, it would provide the first measurements of energy scale of symmetry breaking and of the energy scale of Grand Unified Theory (GUT).

**Key words:** cosmic strings; galaxies: general; cosmology: gravitational lensing

## 1 INTRODUCTION

The Capodimonte - Sternberg - Lens candidate n.1 (or CSL-1) is a peculiar object discovered in the OACDF (*Osservatorio Astronomico di Capodimonte - Deep Field*): a medium-deep multicolour imaging survey covering in three broad and in several intermediate-width bands a  $0.5 \times 1$  deg wide field located at high galactic latitude. The OACDF data were collected at La Silla, Chile, using the Wide-Field Imager at the ESO-MPI 2.2m telescope. An additional set of frames in the  $H$  band filter were taken in March 2002 at the Telescopio Nazionale Galileo (TNG) with the Near Infrared Camera and Spectrograph (NICS). In Table 1 we summarize the most relevant information on the OACDF. More details on the OACDF data reduction and calibration can be found in Capaccioli et al. (2001), and Alcalá et al. (2002).

The photometric criteria listed in Schneider et al. (1992) as rules of thumb for identifying gravitational lens candidates, i. e. the presence of at least two images with small (few arcsecs) angular separation and having the same flux ratio in different spectral bands, were applied to the OACDF first visually and then on the matched catalogues, leading to the identification of several faint gravitational lens candidates. After the rejection of a few spurious objects, the list of candidates was reduced to four objects (named by us

Filter	Exp. Time [hours]	PSF [arcsec]	Phot. Err.
(1)	(2)	(3)	(4)
B	2.0	1.14	$\pm 0.11$
V	1.7	1.01	$\pm 0.13$
R	3.3	0.98	$\pm 0.21$
H*	0.33	0.85	$> 0.2$
753 nm	6.5	0.87	$\pm 0.11$
770 nm	6.0	0.86	$\pm 0.12$
791 nm	6.5	0.97	$\pm 0.12$
914 nm	5.6	0.79	$\pm 0.13$

\* The H band covers only the CSL-1 region

**Table 1.** Characteristics of OACDF. Column 1: photometric broad bands and effective wavelenghts for narrow bands; column 2: total exposure time of the final co-added image [in hours]; column 3: FWHM of the resulting PSF [in seconds of arc] measured in proximity of CSL-1; column 4: relative photometric accuracy measured at the completion limit.

Capodimonte-Sternberg Lens candidates or CSL-1, CSL-2, etc ...).

So far, the spectroscopic follow-up's needed to confirm or disprove the gravitationally lensed nature of the objects

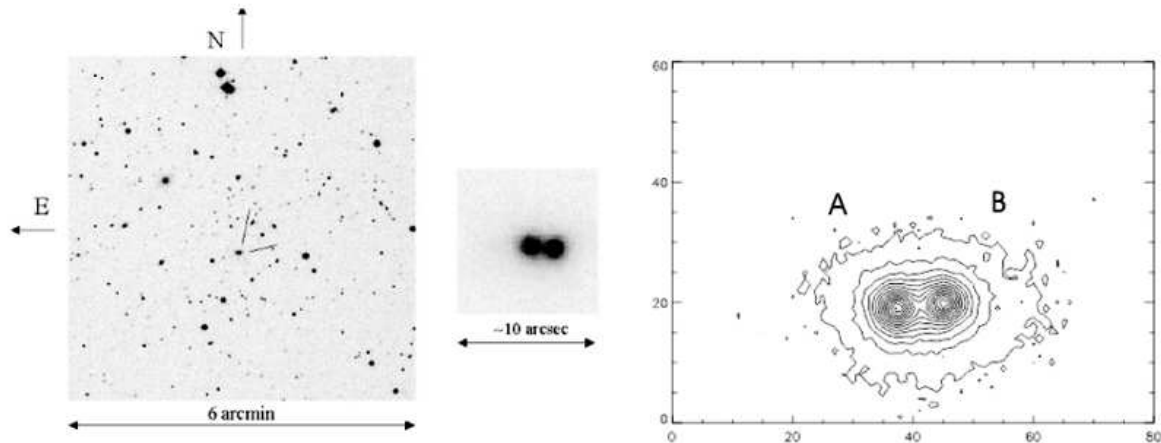


**Figure 1.** Left panel and central inset: appearance of CSL-1 in the R band. Right panel: 2D contours of CSL-1 from the near IR ( $\lambda 914$ ) image. Coordinates are in pixels ( $1 \text{ px} = 0''.238$ ) and the two components are labeled A and B as in the text.

Band	FWHM A [arcsec]	FWHM B [arcsec]	FWHM PSF [arcsec]	mag A	mag B	$r_e^A$ [arcsec]	$\frac{r_e^A}{r_e^B}$
B	1.59	1.67	1.14	$22.73 \pm .15$	$22.57 \pm .15$		
V	1.59	1.67	1.01	$20.95 \pm .13$	$21.05 \pm .13$	6.3	1.4
R	1.98	1.98	0.98	$19.67 \pm .20$	$19.66 \pm .20$	3.0	2.5
H	1.19	1.11	0.85				
A753	1.11	1.19	0.87				
A770	1.27	1.27	0.86			7.4	0.6
A791	1.67	1.59	0.97				
A914	1.27	1.27	0.79			8.8	1.4

**Table 2.** FWHM, magnitudes and effective radii for the two components of CSL-1. Column 1: photometric band; column 2 and 3: FWHM size of component A and B, respectively; column 4: FWHM of the PSF measured in a region close to CSL-1; column 5 and 6: integrated magnitudes of components A and B respectively. These values are provided only for the bands where accurate absolute photometry could be performed. Column 7 and 8: effective radius for the A component and ratio of the effective radii for the two components, respectively. These values are provided only for those bands where the profile was extended enough to allow a reliable fit to a de Vaucouleurs law.

could be performed only for the first candidate (CSL-1), which turned out to be a rather interesting case.

This paper is structured as follows: in Section 2 we summarize the measured photometric and spectroscopic properties of CSL-1 and in Section 3 we discuss the possible explanations of the observables. In Section 4, after introducing some aspects of the string phenomenology, we present our model for the lensing by a cosmic string and the simulation performed in order to assess whether it may explain the strange properties of CSL-1. Finally, in Section 5 we summarize our results and discuss possible future observations.

## 2 THE OBSERVED PROPERTIES OF CSL-1

### 2.1 Morphological and photometric properties

CSL-1 consists of two sources (A and B, as marked in Fig. 1) separated by 1.9 arcsec. Visual inspection shows that in all bands, the two sources have (within the errors) the same

morphology: a bright nucleus surrounded by a faint halo with undistorted and almost circular isophotes.

In Table 2 we list, in each of the OACDF broad bands, the measured FWHM of the two components together with the FWHM of the PSF measured on non-saturated stars near the position of CSL-1. Also in Table 2 we give the integrated magnitudes of the two components in the various bands. It is apparent that, within the errors, the colors of the two components are identical.

In order to investigate the light profile, we performed a two dimensional fit of the observed light distribution with a 2-D Sersic profile  $I_S(r) = I_0 \exp(-b(\frac{r}{r_c})^{1/n})$  convolved with the measured PSF, where:

$$r^2 = \frac{1+e}{2}(x^2+y^2) + \frac{1-e}{2}(x^2+y^2)\cos 2\psi + \frac{1-e}{2}xy \sin 2\psi$$

$x$  and  $y$  being the Cartesian coordinates measured from the central peak,  $e$  the ellipticity of the corresponding isophote, and  $\psi$  the position angle of the isophote. The best fit was obtained for  $n = 4$ , id est for a “de Vaucouleurs” (1948) law.

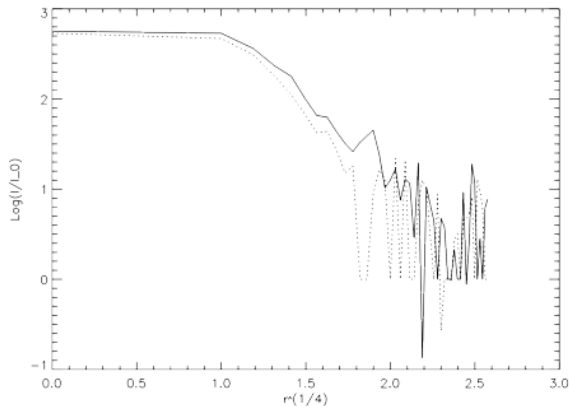


**Figure 2.** Surface brightness profiles obtained for the components A (dashed line) and B (solid line) in the 914 Å band. The profiles are normalized to the peak intensity and plotted in  $r^{1/4}$  units.

Equipment	Exp. time (hours)	Spect. resol.	Spectral range Å
TNG + Dolores	1	12 Å	5200 - 7600
NTT + EMMI	2	9.4 Å	4000 - 8500

**Table 3.** Spectroscopic material. Column 1: telescope and spectrograph; column 2 total exposure time [in hours]; column 3: spectral resolution measured by the FWHM; column 4: covered spectral range.

In Fig. 2 we show the surface brightness profiles obtained for the two components in the 914 Å band; in ordinate we have the logarithm of the surface brightness normalized to the peak value, while the abscissa is in  $pixel^{1/4}$ . The slopes of the linear parts of the two profiles are identical within the errors. For those bands where the surface brightness profile covered a large enough range in magnitudes we also attempted to derive estimates of the effective radii of the two components (see 2). These values, however, suffer of very large errors due to the intrinsic faintness of the source and to the inadequate sampling attained in some bands, and therefore must be regarded as indicative only.

The two dimensional fit was also used to produce a residuals map ( $observed - model$ ) of the light distribution which did not show any systematic trend, with the possible exception of a very faint light excess on the East side. We wish to stress, however, that even in our deepest images ( $R_{lim} \simeq 24.5$ ) we could not detect any residual light in between the two images (see Fig. 8).

Finally, we wish to emphasize that the fainter isophotes of the two components, even though very noisy, have, within the errors, almost identical shapes.

## 2.2 Spectral properties

We obtained two sets of long-slit spectra (with the slit aligned along the direction joining the two images) of both components of CSL-1. The first one was obtained at the Telescopio Nazionale Galileo (TNG) under non photometric

conditions and therefore could not be calibrated, while the second one was obtained at the ESO-New Technology Telescope (NTT) in photometric conditions (cf. Table 3) and the spectrophotometric standards Hiltner 600 and Eg274 were also observed. Spectra were reduced using standard IRAF routines and the sky was removed using the AFI package (Lorenz et al. 1993).

In Figure 3 we show both sets of spectra after applying - for visualization purposes only - a slight vertical shift to the spectrum of component A with respect to the spectrum of component B. In the figure we also mark the position of the most significant features which could be identified. No emission lines could be detected in any of the available spectra.

The cross correlation between the spectra of the two components in the same exposure, gives a differential radial velocity of  $27 \pm 25$  km/s, and the redshift is  $z = 0.46 \pm 0.008$  (independently from both data sets).

The small difference which is observable in the vicinity of Ca line, is very likely instrumental. In order to show the correspondence between the two spectra, in Figure 3 we also show the ratio of the spectra of the two components, which, within the errors is equal to 1 over the whole spectral range. In Fig.4 we show the correlation function of the two spectra, which confirms that the spectra are identical with a confidence level higher than 99.9%.

## 2.3 Putting all together

The available photometric and spectroscopic data suggest that both components of CSL-1 are early-type galaxies at a redshift  $z = 0.46$ . We wish to stress that at such a distance (with  $H_0 = 65$  km/s/Mpc, the distance is  $\sim 1.9$  Gpc), the lower limit for the linear separation between the two objects would be  $\sim 20$  Kpc. In Table 2 we give the absolute magnitude in each band and the estimate effective radii for component A (component B has identical values). All these facts converge in identifying the two images of CSL-1 as giant elliptical galaxies.

Whether the two components of CSL-1 are two identical ellipticals which happen to lay almost along the same line of sight, or rather two images of the same background object produced by a gravitational lens is much more difficult to disentangle. Here we just want to emphasize that the lack of any excess light in between the two images, implies that, if CSL-1 is a lensed object, then the lens is invisible and should be a very peculiar “dark” one (cf. Jackson et al. 1998) which, furthermore, does not distort the overall morphology of the lensed object.

As we shall demonstrate in Section 5, the only gravitational lens able to produce such a morphology is a cosmic string but, before examining this odd possibility, we need to rule out or at least investigate all other possible, even though equally unlikely, alternatives.

## 2.4 CSL-1 as a peculiarly obscured object

The observed morphology could be the result of obscuration by a gigantic strong dust lane. There are several reasons which allow, however, to reject this hypothesis. First of all, with a minimum separation between the two sources of 20

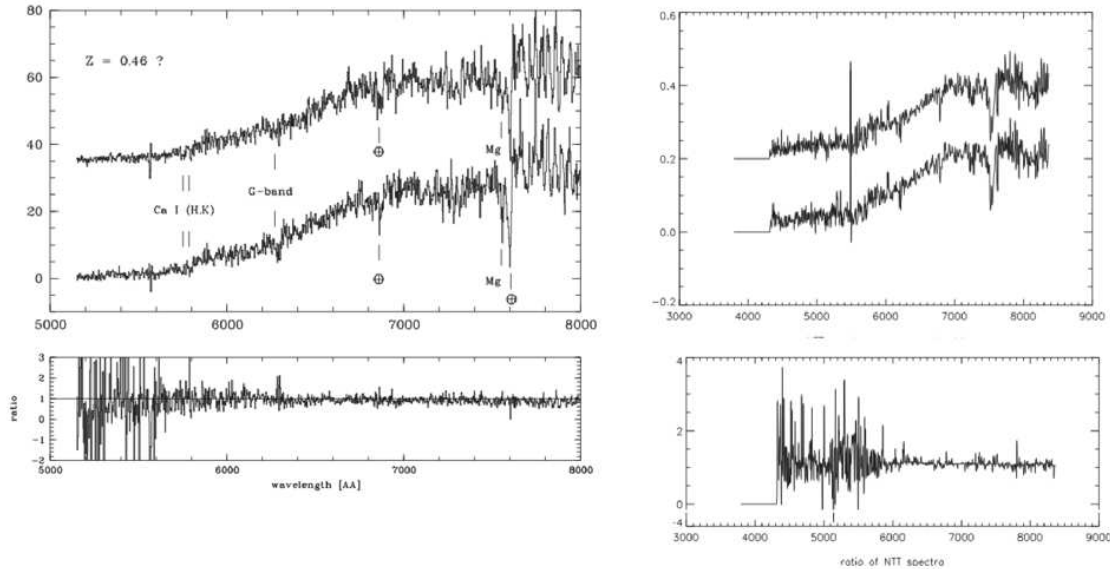


**Figure 3.** Left panel: TNG spectra of the components of CSL-1 . Right panel: NTT spectra. A vertical shift was introduced for visualization purposes only. Lower panels: corresponding ratios obtained by dividing the spectra of the two components.

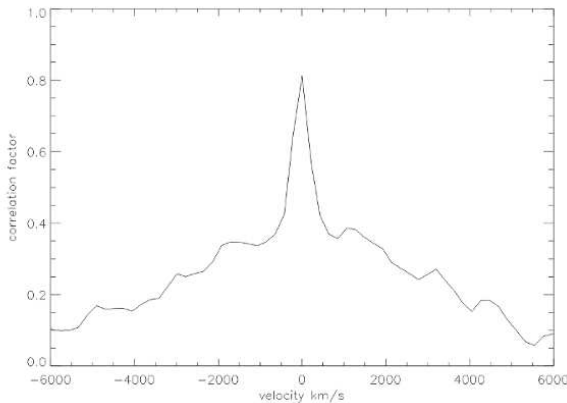


**Figure 4.** Correlation coefficient of NTT spectra of the two components of CSL-1 with background profile removed.

Kpc, it would be by far the largest such structure ever observed; second, in order to produce identical and symmetric sources it should have a perfectly tailored shape. Furthermore, even in such unlikely case, such an obscuring layer would fail to reproduce the light profiles observed at the various wavelengths.

To prove it quantitatively we performed a simple simulation. The underlying hypothetical galaxy was modeled assuming, as previously done, a de Vaucouleurs profile and for the dust lane a standard absorbing law given by  $\exp(-\tau(x))$ , where  $x$  is the coordinate along the profile and  $\tau$  is the geometry factor describing the distribution of dust at a given  $x$ :  $\tau(x) = \frac{f(x)}{\lambda^n}$ . In this formula,  $n$  is the so called dust index (cf. Hildebrand (1983); Ferrari (2002); Chini (1984)) which, from optical to radio, assumes values inside the range  $1 \div 2$ . The above formulae allow us to derive the light profile to be expected in any given band relative to the  $R$  frame assumed as template. In Figure 5 we show the expected and the ob-

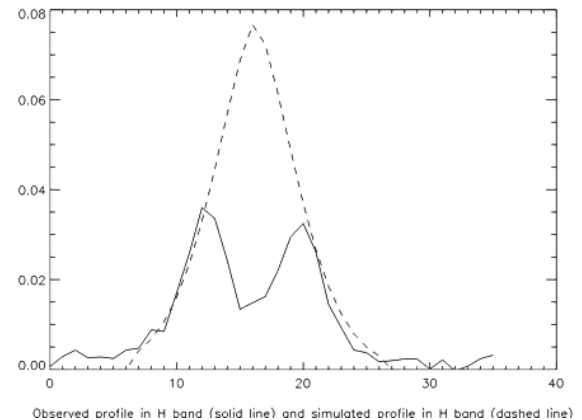


**Figure 5.** Solid line: observed H band profile for CSL-1 ; dashed line: profile expected in the H band following the procedure described in the text (dust index  $n=1$ ).

served H profiles for a dust lane capable to reproduce the dip observed in the R profile.

As an additional test, in order to investigate whether the combined effects of dust extinction and very strong colour gradients could reproduce the observed morphology, we measured colour in the wings and between peaks of the B, V, and R profiles. The results show that colour gradients, if present, are smaller than 0.1 mag and therefore are of no help in explaining the observed morphology by means of a dust lane.

Therefore we are left with only two possible explanations for CSL-1 . Either we are dealing with i) the projection of two giant elliptical galaxies which are identical (at a 99% level of confidence) in terms of magnitudes, colours, morphology and, what is more relevant, also in terms of spectral properties, or ii) we are seeing the effects of an

unconventional and so far never observed gravitational lens which does not distort extended images.

### 3 CSL-1 AS A GRAVITATIONAL LENS

#### 3.1 Compact lens models

The peculiar properties of CSL-1 cannot be explained in terms of lensing by a compact lens such as, for instance, the models listed in the Keeton catalogue of models (Keeton 2002). As a template case, let us take into consideration that of a Singular Isothermal Sphere (SIS), id est the most commonly used (and reliable) model for a gravitational lens. In Fig.6 (left panel) we show the results of the simulation of a SIS lensing effect for an extended object: as it can be easily seen, the SIS model produces a distortion of the outer isophotes. The simulation was performed as follows: we assumed a "de Vaucouleur"-like 2D light distribution and then mapped it to the lens plane accordingly to the gravitational field generated by a SIS. Afterwards, the modelled image was smoothed with the observed Point Spread Function and a realistic (id est with the same statistics of the real image) noise was added. As optimization value we took the difference between the observed and modelled images squared and optimized over the parameters of the light distribution and of the SIS. The distortions introduced by the SIS are clearly visible. In Fig.6 (right panel) we show the residuals between the modelled and observed images: as it can be seen, the residuals exceed by  $5\sigma$  the noise level. This behavior of the residuals is confirmed also by the analysis performed in all other available bands and we wish to stress that, since in different bands the noise is uncorrelated, the residuals may be considered as independent events and, therefore, the composite probability of having the same fluctuations in the same positions is absolutely negligible.

Furthermore, in the unlikely case of ordinary lensing by a massive object, one could also estimate some characteristics of the lens. First of all we can restrict the redshift range for the lens inside  $0.1 < z < 0.4$ . The velocity dispersion (mass parameter for a SIS lens) should therefore be in the range 200 km/s up to 400 km/s. Such value is typical of a giant galaxy and therefore, if we assume a lens made of ordinary matter, it should be clearly visible in our images which is not a case. Therefore one have to suppose that it is a case of dark lens. As stressed above, such a "dark" gravitational lens, while being completely invisible, would introduce significant and measurable distortions in the lensed images (producing arc-like features) which are not observed in CSL-1.

#### 3.2 Cosmic string model

Cosmic strings were introduced in theoretical cosmology by Kibble (1976), Zeldovich (1980), Vilenkin (1981), Gott (1985), de Laix et al. (1996), Bernardeau et al. (2001). Vilenkin (1981) also suggested that they could be revealed by means of gravitational lensing phenomena.

From a physical point of view, a cosmic string is characterized by a mass per unit length  $\mu$  and by a tension  $T = \mu$  along the string. Therefore, a string has only one parameter defining both its microscopic physical properties and

the macroscopic properties of the surrounding space-time. The microscopic characteristic of the string is the diameter, which is of the order of the square root of  $\mu^{-1}$ . Below we shall use Planck units, so that  $\mu = 1$  corresponds in usual units to  $1.4 \cdot 10^{28}$  g/cm and the diameter of a cosmic string would be of the order of  $10^{-33}$  cm. All modern theories, however, predict  $\mu \ll 1$  thus implying a larger but still microscopic value for the expected diameter of a string. We can therefore safely assume that, on a cosmic scale, the diameter of the string can be neglected with respect to all the other linear quantities involved.

From the lensing point of view, a cosmic string produces a conical space time where the cusp of the cone coincides with the position of the string. The complete turn in a plan perpendicular to the string gives the total angle  $\Phi$  (smaller than  $2\pi$ ). The difference  $2\pi - \Phi$  is called "angle deficit" and it is defined by the string density:

$$D = 8\pi\mu \quad (1)$$

in the case of  $\mu \ll 1$ . In order to understand the lensing properties of a cosmic string let us assume the following geometry: a distant point-like source (for instance a QSO) and a cosmic string interposed along the line of sight and at rest with respect to the observer. Let the angular cosmological distance from the observer to the string be  $R_s$  and that between the QSO and the observer  $R_q$ . If the angular distance between the QSO and the string (as seen from the observer) is less than  $D$ , then the observer sees two images of the QSO separated by the angle (Gott, 1985):

$$\Delta\theta = D \sin \alpha \frac{R_q - R_s}{R_q}, \quad (2)$$

where  $\alpha$  is the angle between the string and the vector coinciding with the observer and the point source.

In what follows we shall assume for simplicity that  $R_s \ll R_q$  and  $\alpha = \pi/2$  that is  $\Delta\theta = D$ . The proper distances depend on the cosmological model (we shall assume a standard cosmological model: FRW metric with flat space  $\Omega_{tot} = 1$ , and  $\Omega_\Lambda = 0.7$ ,  $\Omega_{CDM} = 0.3$  according to modern measurements de Bernardis et al., (2002)). When the source is still far away from the string, no lensing is induced and the image is unperturbed, while when the angular separation reaches  $D$ , the lensing phenomenology sets in and a second image of the source begins to form on the opposite side of the string, at an angular distance  $D$  from the source position. We wish to stress that, on the contrary of what happens in other lensing models, the lensing by a cosmic string does not introduce any amplification of the signal from the background source.

In Figure 7 we show (as 3-D light distribution and as isocontours) the results of our simulation of the observed photometric properties of CSL-1 in the band  $\lambda = 914 \text{ \AA}$ . As before, the background source was modelled using de Vaucouleurs law. The figure gives the outcome of the simulation for two different seeing: the observed one and a 40 milliarc-sec seeing assumed to be representative of the HST average operating conditions. Finally, in Figure 8 we plot the isocontours for the residuals (observed - modelled) of our best fitting model. No systematic trend can be observed. As it can be seen, lensing by a cosmic string should produce a characteristic signature consisting in isophotes with very sharp edges. This signature, however cannot be observed under

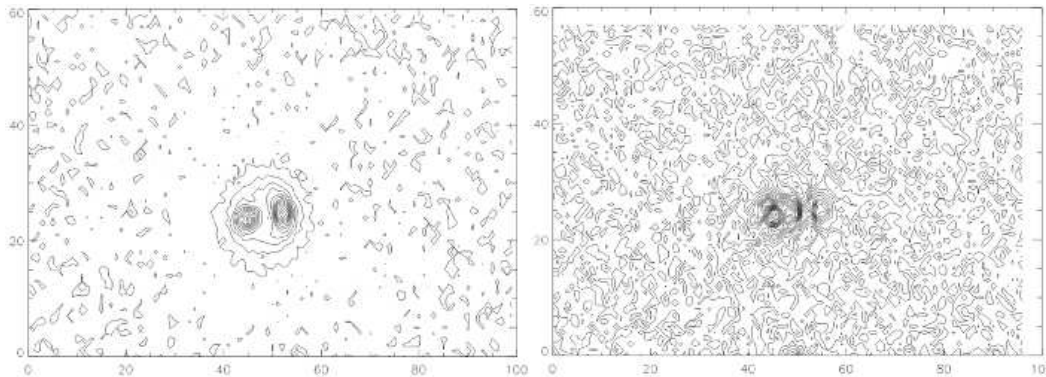


**Figure 6.** Left: contours of the primary and secondary images in the case of an optimal SIS lens in the band 914 Å. The images are convolved with PSF of the band. The distortion of the outer isophotes is clearly visible. Right: residuals (modelled - observed) for the 914 Å image.

average seeing conditions. In fact, if the seeing FWHM is comparable with the size of the secondary image (as it is the case for our data), the observer sees smooth and nearly circular images with the secondary one slightly fainter.

#### 4 DISCUSSION AND CONCLUSIONS

As discussed above, the optical morphology of the candidate lens CSL-1 can be explained in terms of lensing by a cosmic string. Even though this may seem unlikely due to the expected rarity of such strings and to the fact that on the basis of present observational evidence we cannot yet rule out the only other (also unlikely) possible explanation in terms of projection effects, we want to stress that, if confirmed, this would be the first clear cut evidence ever for a cosmic string, and would therefore have a far reaching impact in both cosmology and particle physics. There is, however, an easy way to disentangle between the two possible explanations. As shown above, a cosmic string would introduce a clear cut signature in the shape of the lensed object which can be detected in high angular resolution optical data. In the case of positive detection, the parameters derived for the cosmic string will allow us to determine its linear density and thus measure the energy scale of symmetry breaking and of the energy scale of Grand Unification Theory (GUT).

Observation in radiofrequency bands would also be needed. A straight long string induces temperature fluctuation on the cosmic microwave background radiation, and is therefore expected to produce a linelike discontinuity at the place of the string. The amplitude of fluctuation is given by Kaiser and Stebbins (1984):

$$\frac{\delta T}{T} \approx 8\pi\mu v$$

here  $v$  is the velocity of string perpendicular to the line of sight in the units of light velocity. Usually the velocity of cosmic string is expected to be close to unity due to stresses which are inside the string. If the velocity is close to unity, one can expect significant anisotropy which will form a strip of  $\delta T/T$  along the position of the string with angular width of the order of  $2''$  and amplitude  $\sim 30 \mu\text{K}$ . This strip would cross the optical images of CSL-1 perpendicularly to the line connecting the two components. Although the expected

angular scale is very small, the amplitude is easily detectable with modern radiometers (see, for instance, de Bernardis et al. (2002)).

If we accept the interpretation of CSL-1 as a gravitational lens produced by a cosmic string, it is possible to derive the scale of energy at which the symmetry breaking occurred. The physical mechanism which produces cosmic strings is related to the phase transition in the early Universe: cf. Gott, (1985) and Dolgov Sazhin and Zeldovich, (1990). This phase transition took place when the temperature of the Universe fell below a critical temperature defined by some energy scale which, on the other end, defines the unification of physical interactions, and, probably, also the main parameters of the inflation. The distance between the peaks of the two images  $\sim 2''$  of CSL-1 roughly corresponds to the "deficit angle"  $D$ . One can therefore estimate the density of the string as  $4 \cdot 10^{-9} m_{pl}^2$ , or in CGS physical units  $5.4 \cdot 10^{21} \text{ g/cm}$ . This value, if our interpretation of CSL-1 is correct, may be used to estimate many physical parameters.

For grand unified strings one can expect

$$\mu \sim \frac{m^2}{\alpha} \quad (3)$$

where  $\alpha$  is a running coupling constant and  $m$  is the typical mass scale of the symmetry breaking. Particle physicists believe that symmetry breaking took place at an energy scale of the order of  $E \sim 10^{16 \pm 0.3} \text{ GeV}$ . This value is derived from the extrapolation of accelerators data Klapdor-Kleingrothaus, and Staud, (1995). Near this scale, all running coupling constants of physical interactions merge, and the value of united coupling constant is:

$$\alpha^{-1} = 25.7 \pm 1.7 \quad (4)$$

Taking into account (3) and (4) and the value of the deficit angle derived from our data, one can estimate the mass scale of symmetry breaking as  $2 \cdot 10^{15} \text{ GeV}$ , which is in reasonable agreement with extrapolated accelerators data.

#### ACKNOWLEDGEMENTS

M.V. Sazhin acknowledges the Capodimonte Astronomical Observatory for hospitality and financial support, also acknowledges the financial support of RFFI grant 00-02-16350.

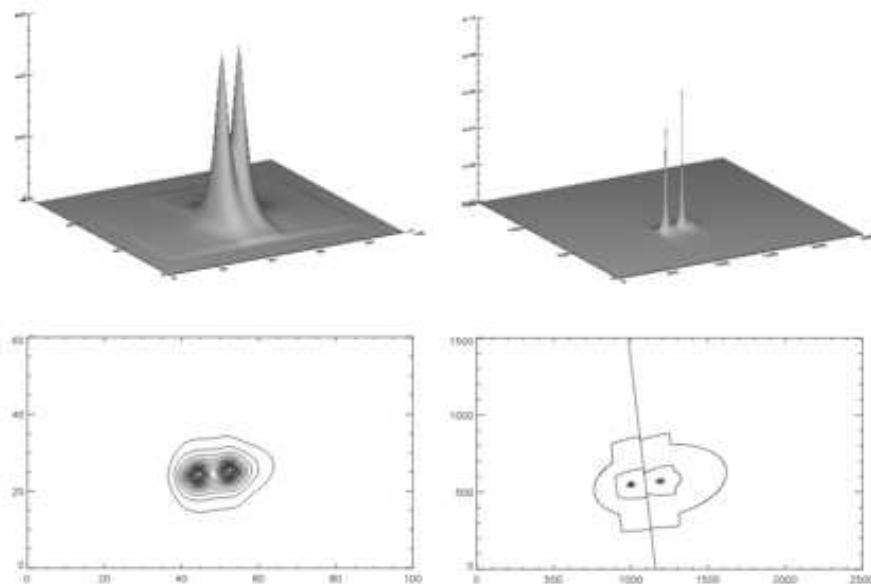


**Figure 7.** Upper left and lower left panels: 3-D light distribution and isophotal contours obtained after convolving our model with the observed PSF. Upper right and lower right panels: the same but convolving for an HST like PSF with a FWHM of 40 milliarcsec.

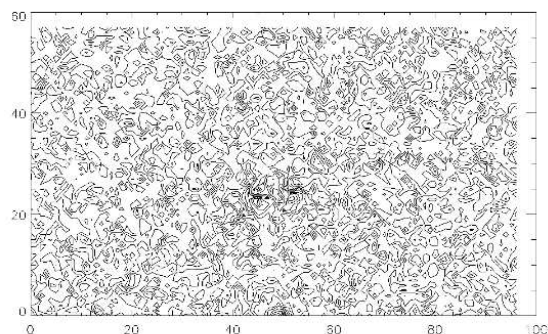


**Figure 8.** Contours of the residuals (observed - modelled) for the light distribution of CSL-1 (in the 914 nm band). The maximum value of the residual is  $2\sigma$  above the background.

This research was partly funded by the Italian Ministry for Public Instruction, University and Research through a COFIN grant. Authors are also indebted to G. Busarello for fruitful discussions and to the ESO and TNG staff for support during the observations.

## REFERENCES

- Alcalá J. M., Radovich M., Silvotti R., et al., in Proc. of the SPIE Meeting on *Survey and other telescope technologies and discoveries*, Waikoloa-Hawaii, 2002, in press
- Bernardeau F., Uzan J.-P., 2001, Phys.Rev D, 63, 023004, 023005
- Capaccioli M., Alcalá J.M., Silvotti R., et al., ESO Press Release 15a-f/01, <http://www.eso.org/outreach/press-rel/pr-2001/phot-15-01.html>
- Chini R., Mezger P.G., Kreysa E., et al., 1984, A. & Ap., 135, L14; 137, p.117
- de Bernardis et al., 2002, ApJ, 564, 559
- de Laix A.A., Vachaspati T., 1996, Phys.Rev. D, 54, 4780
- de Vaucouleurs G., 1948, Ann. d'Astrop., 11, 247
- Dolgov A., Sazhin M., Zeldovich Ya., 1990, *Basics of Modern Cosmology*, Frontieres:France
- Ferrari F., Pastoriza M.G., Macchetto F.D., et al., 2002 A. & Ap., in press (astro-ph-0204431)
- Gott III J.R., 1985, Ap. J., 288, 422
- Hildebrand R.H., 1983, Quarterly J. R. Astron. Soc., 24, 267
- Jackson N., Helbi P., Browne I., et al., 1998, A. & Ap., 334, L33
- Kaiser N., Stebbins A., 1984, Nature, 310, 391
- Keeton Ch., 2002, , <http://cfa-www.harvard.edu/castles/Kibble>
- Kibble T.W.B., 1976, J. Phys. A: Math. & Gen., v.9, p.1387
- Lorenz H., Richter G.M., Capaccioli M., Longo G., 1993, A. & Ap., 277, 321
- H.V. Klapdor-Kleingrothaus, and A.Staud, "Teilchenphysik ohne Beschleuniger", B.G. Teubner:Stuttgart, 1995.
- Schneider P., Ehlers J., Falco E.E., Gravitational Lenses, 1992, Springer: Heidelberg
- Vilenkin A., 1981, Phys. Rev. D, 23, 852
- Zeldovich Ya. B., 1980, MNRAS, 192, 663